Multipole-Based Cable Braid Electromagnetic Penetration Model: Magnetic Penetration Case

Salvatore Campione[*], Larry K. Warne, and William L. Langston

Abstract—The goal of this paper is to present, for the first time, calculations of the magnetic penetration case of a first principles multipole-based cable braid electromagnetic penetration model. As a first test case, a one-dimensional array of perfect electrically conducting wires, for which an analytical solution is known, is investigated: we compare both the self-inductance and the transfer inductance results from our first principles cable braid electromagnetic penetration model to those obtained using the analytical solution. These results are found in good agreement up to a radius to half spacing ratio of about 0.78, demonstrating a robustness needed for many commercial and non-commercial cables. We then analyze a second set of test cases of a square array of wires whose solution is the same as the one-dimensional array result and of a rhomboidal array whose solution can be estimated from Kley's model. As a final test case, we consider two layers of one-dimensional arrays of wires to investigate porpoising effects analytically. We find good agreement with analytical and Kley's results for these geometries, verifying our proposed multipole model. Note that only our multipole model accounts for the full dependence on the actual cable geometry which enables us to model more complicated cable geometries.

1. INTRODUCTION

The topic of electric and magnetic penetrations through shielded cables is of great importance and has a long history, including solid shields [1], cable braids and shielding [2–5], porpoising effects [6], and low-frequency diffusion [7].

This paper focuses on reporting for the first time calculations of the magnetic penetration case of the rigorous cable braid penetration model discussed in [8–10] for perfect electrically conducting wires. Transmission line models are often used to model shielded cables. Sample per-unit-length cells for shield and inner conductor transmission lines of a single-shield cable are provided in Fig. 1. The shield properties are modeled via the per-unit-length impedance and admittance parameters Z_{sh} and Y_{sh} as in Fig. 1(a). Because of electric and magnetic field penetrations, currents and voltages are induced on the inner conductor, modeled via the per-unit-length self-impedance Z_c and the self-admittance Y_c in Fig. 1(b), which are formed by the inner conductor and the shield. The penetration mechanisms are modeled via the per-unit-length transfer impedance Z_T (proportional to the transfer inductance L_T) and the per-unit-length transfer admittance Y_T (proportional to the transfer capacitance C_T) in the form of distributed voltage and current generators as in Fig. 1(b). All these transmission line parameters take into account the braid weave characteristics and material of the shielded cable [2–5, 8, 9, 11].

In [12], we have reported a multipole model for the electric penetration to evaluate the per-unit-length transfer capacitance C_T and the per-unit-length self-capacitance C_c. In general, however, it is common for the magnetic penetration to dominate the response of a cable, and is an important topic of investigation. Note that in this paper we limit our investigation to perfect electric conductor wires

* Corresponding author: Salvatore Campione (sncampi@sandia.gov).
The authors are with the Electromagnetic Theory Department, Sandia National Laboratories, Albuquerque, NM 87185, USA.

(a) Shield transmission line   (b) Inner conductor transmission line
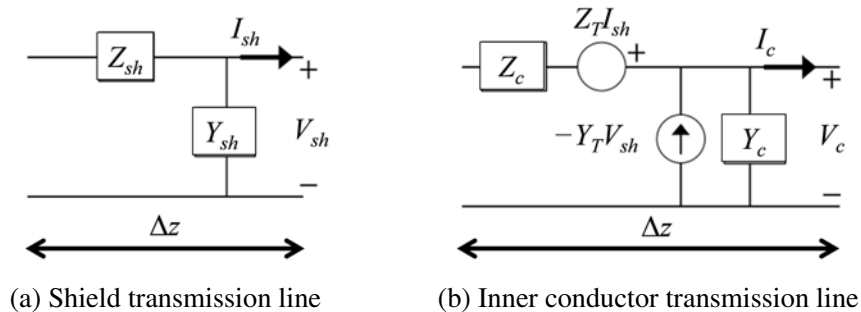
Figure 1. Per-unit-length cells for the (a) shield and (b) inner conductor transmission lines of a single-shield cable.

as a step toward the final braid description including losses arising from finite conductors, which will be included in future work.

Generally, the complete semi-empirical model assembled by Kley [13] based on canonical models augmented by measurements of typical commercial cables is used to estimate C_T and L_T. This model is quite useful and identifies the fundamental penetration mechanisms. However, our goal here is to apply our first principles model [8, 9] that delivers results for L_T and the per-unit-length self-inductance L_c that are dependent on the detailed geometry of the cable in question. In turn, this would allow the modeling of cables that deviate from typical geometries employed in commercial cables.

The paper is structured as follows. We summarize in Sec. 2 the first principles model based on multipoles for magnetic penetration, discussing both co-location and Galerkin approaches. We then apply in Sec. 3 our first principles model to a canonical structure, namely a one-dimensional array of wires, which can be modeled analytically. Then, in Sec. 4, we devise a square array test case whose solution can be constructed through the one-dimensional array result. We further analyze a rhomboidal array test case whose solution is estimated via Kley's model. We also investigate porpoising effects in Sec. 5 through the analysis of a structure made of two layers of one-dimensional arrays of wires. All the results here reported verify the correctness of the proposed first principles multipole model for magnetic effects.

2. MULTIPOLE MODEL FOR MAGNETIC PENETRATION

The cable penetration model is based on finite-length magnetic line multipoles. In general, increasing the number of multipoles provides more means to model the magnetic charge distribution in each of the wire segments, and leads to more accuracy at the cost of more complicated multipole moment formulas.

We set up the magnetic braid problem in a manner similar to the electric problem reported in [12] through a combination of the filament magnetic vector potential $\underline{A}_f$ (used to represent the net current carried by each braid wire) and magnetic scalar potential ϕ_m (used to match the boundary conditions on the wire surface). The magnetic induction $\underline{B}$ and magnetic field $\underline{H}$ are given by

$$\underline{B} = \mu_0 \underline{H} = -\mu_0 \nabla \phi_m + \nabla \times \underline{A}_f, \tag{1}$$

where μ_0 is the absolute permeability of free space. We consider the situation where the region above the wires represents the inner region of the cable.

The magnetic flux Φ through a surface S, bounded by contour C, from this representation is given by

$$\Phi = \oint_C \underline{A}_f \cdot \underline{dl} - \mu_0 \int_S \nabla \phi_m \cdot \underline{n} dS. \tag{2}$$

which then is used to define the transfer inductance as $L_T = \Phi/H_0$ [14], where Φ is the magnetic flux per unit length passing between the wires and the point $y \to +\infty$ and the drive uniform magnetic field in the planar problem below the wires is $\underline{H}_{inc} = H_0 \underline{x}$ ($y = 0$ is at the center of the structure; note that

$\underline{x}$ is a unit vector in the x direction, and $\underline{n}$ is a unit vector normal to the surface S). A similar definition can be introduced for the self-inductance L_c exciting the cable from above.

The magnetic scalar potential is here represented by a magnetic multipole summation similar to the electric problem [12] and by a magnetic current filament (and the field given by the magnetic vector potential). The solution for a varying magnetic line charge $q_m(z)$ is

$$\phi_{scatt} = \frac{1}{4\pi\mu_0} \int q_m\left(z'\right) \frac{dz'}{|\underline{r}-\underline{r}'|}. \tag{3}$$

It is efficient to represent the magnetic scalar potential ϕ_m by a magnetic multipole summation to capture the transverse field behavior. The potential for an axially varying line charge $q(s)$ discretized as pulses of strength q_n is (where s is the axial coordinate along segment n and ρ is the transverse coordinate [8, 9])

$$\phi_{scatt} = -\sum_{n=1}^{N} \frac{q_n}{4\pi\mu_0} \ln\left[\frac{(s-s_n/2)+\sqrt{\rho^2+(s-s_n/2)^2}}{(s+s_n/2)+\sqrt{\rho^2+(s+s_n/2)^2}}\right]. \tag{4}$$

Following the steps in [8, 12], we include a series of line multipole moments in the potential, which for a given position n, is written as

$$\phi_{scatt}^n = \frac{-1}{4\pi\mu_0} \sum_{m=0}^{M} \underline{p}^{(0)}\underline{p}^{(1)}\cdots\underline{p}^{(m)} \cdot \nabla_t^m \ln\left[\frac{(s-s_n/2)+\sqrt{\rho^2+(s-s_n/2)^2}}{(s+s_n/2)+\sqrt{\rho^2+(s+s_n/2)^2}}\right], \tag{5}$$

and the total potential is $\phi_{scatt}^{tot} = \sum_{n=1}^{N} \sum_{j=-\infty}^{\infty} \sum_{k=-\infty}^{\infty} \phi_{scatt}^n$, with ∇_t the "del" operator transverse to the particular wire segment. The final matching equation to determine the $2M$ multipole moments (which are transverse vector components: $M+1$ even moments and $M-1$ odd moments in the azimuth about the wire segment) on each of the N segments of the braid wires imposes one of the following conditions:

$$\underline{n} \cdot \underline{H} = 0 = \underline{n} \cdot \left(-\mu_0\nabla\phi_m + \nabla\times\underline{A}_f\right), \text{ (Co-location)}$$

$$0 = \int_0^{2\pi} \underline{n} \cdot \left(-\mu_0\nabla\phi_m + \nabla\times\underline{A}_f\right)\left(\begin{array}{c}\varepsilon_m\cos\left(m\phi\right)\\-2\sin\left(m\phi\right)\end{array}\right) d\phi, \text{ (Galerkin)} \tag{6}$$

with $\underline{n}$ the radial vector to the wires, and

$$\underline{A}_f = \frac{\mu_0}{4\pi} \sum_{n=1}^{N} \sum_{j=-\infty}^{\infty} \sum_{k=-\infty}^{\infty} I_n\underline{e}_{sn} \ln\left[\frac{(s-s_n/2-ju_{sn}-kv_{sn})+\sqrt{|\underline{\rho}-j\underline{u}_{\rho n}-k\underline{v}_{\rho n}|^2+(s-s_n/2-ju_{sn}-kv_{sn})^2}}{(s+s_n/2-ju_{sn}-kv_{sn})+\sqrt{|\underline{\rho}-j\underline{u}_{\rho n}-k\underline{v}_{\rho n}|^2+(s+s_n/2-ju_{sn}-kv_{sn})^2}}\right]. \tag{7}$$

The co-location method assumes a number of matching points equal to the number of multipole coefficients (1 for the filament, 3 for the dipole, 5 for the quadrupole, and 7 for the octopole). The Galerkin method has instead N_G integration points around each wire for each multipole order, and $\varepsilon_m = 1$ if $m = 0$ and $\varepsilon_m = 2$ otherwise. We implemented a trapezoidal rule to perform the Galerkin integral in Eq. (6), but higher order integration algorithms (e.g., Gauss or Newton-Cotes) could be employed to reduce the number of required points.

The actual solution technique decomposes the problem of an $H_x = H_0$ magnetic field below the braid and zero magnetic field above the braid as in Fig. 2(a) and the problem of an $H_x = H_0$ magnetic field above the braid and zero magnetic field below the braid as in Fig. 2(b) into the superposition of two problems. The first problem (referred to as Problem A) is setup with an x-directed uniform incident field $H_x = H_0/2$ and zero current on the braid wires as in Fig. 2(c). The second problem (referred to as Problem B) is setup with a zero incident field and a total current I flowing on the wires composing the braid as in Fig. 2(d). The solution to the problem in Fig. 2(a) is then reconstructed by summing the solutions of Problems A and B, while the solution to the problem in Fig. 2(b) is obtained by subtracting the solution of Problem B from the one of Problem A.

(a) Excitation from below

(b) Excitation from above

(c) Problem A
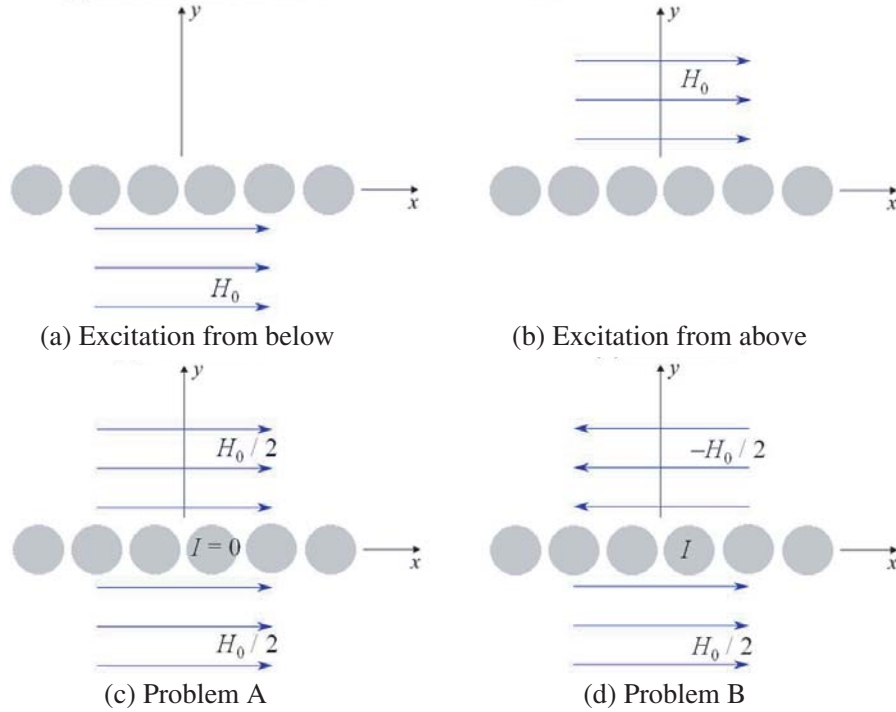
(d) Problem B

Figure 2. The problems of (a) an $H_x = H_0$ magnetic field far below the braid and zero magnetic field far above the braid and (b) an $H_x = H_0$ magnetic field far above the braid and zero magnetic field far below the braid are decomposed into (c) a problem with no wire currents but a symmetric uniform-field $H_0/2$ at large distances, and (d) a problem with distant antisymmetric field $\pm H_0/2$ on the two sides (with the discontinuity supported by the current I).

Through the multipole model, the transfer inductance is computed using

$$L_T = \frac{1}{I_1 I_{sh} \ell} \int\limits_{S_0} \left(\mu_0 \frac{A_{fc}}{B_0} \right) \underline{H}_{sh,0} \cdot \underline{H}_0 dS - \frac{1}{I_1 I_{sh} \ell} \int\limits_{S_w} \underline{A}_{fsh} \cdot \underline{K}_1 dS, \tag{8}$$

where the subscripts "sh" and "1" indicate excitation from below (as in Fig. 2(a)) and from above (as in Fig. 2(b)), respectively, I is a unit cell current, S_0 is a surface far away above the braid, S_w is the wire surface, ℓ is the unit cell period, $\underline{A}_f$ is the filament vector potential, $\underline{K}_1 = -\underline{n} \times \underline{H}_1$, with $\underline{n}$ pointing into the wire center, is the wire current accounting for all the multipolar contributions, and the constant A_{fc}/B_0 is computed via

$$A_{fsh,z} \sim \mu_0 \frac{A_{fc}}{B_0} \underline{e}_z \cdot \left[\underline{n} \times \underline{H}_{sh,0} \right] \tag{9}$$

with $\underline{e}_z$ the segment direction and $\underline{n}$ pointing toward the inner conductor of the cable.

The self-inductance is in general given by $L_c = L_0 + \Delta L_1$, where L_0 is an auxiliary inductance and ΔL_1 is a correction term. The correction to the self inductance is similarly computed through

$$\Delta L_1 = \frac{1}{I_1^2 \ell} \int\limits_{S_0} \left(\mu_0 \frac{A_{fb}}{B_0} \right) \underline{H}_0 \cdot \underline{H}_0 dS - \frac{1}{I_1^2 \ell} \int\limits_{S_w} \underline{A}_{f1} \cdot \underline{K}_1 dS, \tag{10}$$

and the constant A_{fb}/B_0 is computed via

$$A_{f1,z} \sim -\mu_0 \left[\left(\underline{\rho} - \underline{\rho}_m + \underline{n} \frac{A_{fb}}{B_0} \right) \times \underline{H}_0 \right] \cdot \underline{e}_z \tag{11}$$

where $\underline{\rho}$ is the observation position far away and $\underline{\rho}_m$ denotes the average braid position.

3. ONE DIMENSIONAL ARRAY OF WIRES

This section considers the effects of line magnetic multipole additions to the simple filament approximation in representing the elements of a one dimensional wire array, schematically shown in Fig. 3. The case of a one-dimensional array of wires represents a problem that is interesting on its own. The analytic solution for this test case for both transfer and self-inductance checks the basic multipole solution accuracy for shield wires in close proximity but does not include all the characteristics of a braided shield (for which no analytic solution exists).
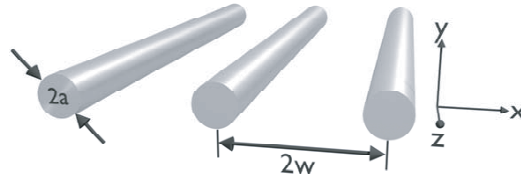
Figure 3. A one dimensional array of wires with period $2w$ along the x direction and radius a. Note the wires are infinitely extended along the z direction.

The array is periodic in x with infinitely extended wires oriented along the z axis with wire spacing $2w$ and wire radius a. We will examine general ratios of wire radius a to wire half spacing w to determine the accuracy of the proposed multipole model.

The multipole model will be compared to an analytical solution developed in [14]. The self-inductance is in general given by $L_c = L_0 + \Delta L_1$, where L_0 is an auxiliary inductance and ΔL_1 is a correction term given by an analytical solution up to the quadrupole term as

$$\frac{2\pi}{\mu_0}\Delta L_1 = -\ln\left[2\sinh\left(\frac{\pi a}{2w}\right)\right] - \left(\frac{\pi a}{2w}\right)\tanh\left(\frac{\pi a}{2w}\right) + \frac{\ln\left\{\sinh\left(\frac{\pi a}{2w}\right)/\sin\left(\frac{\pi a}{2w}\right)\right\}}{1 + \sinh^2\left(\frac{\pi a}{2w}\right)/\sin^2\left(\frac{\pi a}{2w}\right)}. \tag{12}$$

An accurate approximation to the transfer inductance (which holds for all ratios of radius to spacing) uses the exponential decay from the bipolar system of coordinates (representing two cylinders) times the conformal mapping filament array result. The distance $d = O(a) = ca$, with $c = 0.5\sqrt{1 + \pi a/(2w)}$, is taken to represent the termination point for the bipolar decay in the conformal mapping multipole results to account for the missing decay in the filament result, leading to

$$L_{T,bs} \approx -\frac{\mu_0}{2\pi}\ln\left(1 - e^{-\pi a/w}\right)\exp\left[-2\pi\frac{\arctan\left(c/\sqrt{w^2/a^2 - 1}\right)}{\ln\left(w/a + \sqrt{w^2/a^2 - 1}\right)}\right], \tag{13}$$

with subscript "bs" denoting bipolar solution.

The self- and transfer-inductances from the first principles multipole model [using both co-location and Galerkin boundary conditions in Eq. (6)] are reported in Figs. 4 and 5 versus a/w considering up to order $M = 0$ (filament), 1 (dipole), 2 (quadrupole), and 3 (octopole). Note the actual values a and w are not important because the results are shown versus the ratio a/w, the only parameter the self and transfer inductances depend on as shown in Eqs. (12) and (13). (In our implementation, we fixed $a = 0.0025$ inches and varied w, but this choice is arbitrary. Note we also arbitrarily assume the period along the z-direction to be equal to a.) Solid lines are computed using the co-location boundary condition, while other results are computed using the Galerkin method with $N_G = 7$ and 20 (for the self-inductance) and $N_G = 7$, 20, 50, and 100 for the transfer inductance, respectively. Looking at the co-location results (blue curves), one can see that they provide reasonable but limited accuracy due to the small number of matching points used (the right-hand blue curves in Fig. 5(a) and Fig. 5(c) are invalid co-location results for large a/w). Improved results are obtained when using the Galerkin method, with the number of samples required in the integration depending on the multipole order considered. The self-inductance generally converges quickly, with $N_G = 7$. However, for the transfer
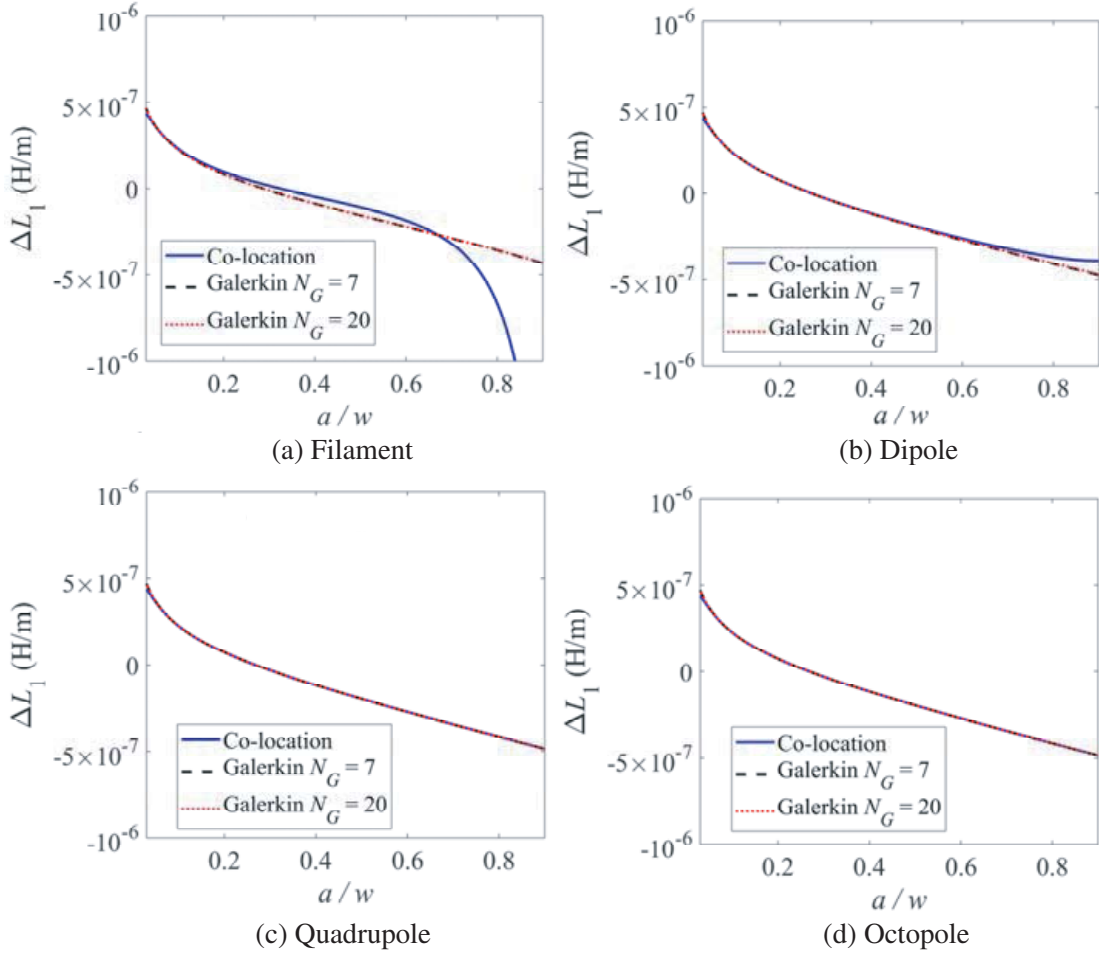
Figure 4. The self-inductance of a one dimensional wire array versus the ratio a/w using the first principles magnetic multipole penetration model up to order (a) $M = 0$ (filament), (b) $M = 1$ (dipole), (c) $M = 2$ (quadrupole), and (d) $M = 3$ (octopole). Both the co-location and the Galerkin method are used here.

inductance, while $N_G = 7$ is enough for the filament term, $N_G = 20$ is required for the dipole, and $N_G = 100$ for the quadrupole and the octopole.

We then compare in Fig. 6 the results using the Galerkin boundary condition with the largest N_G considered for each multipole order in Fig. 5 to the analytical solutions in Eqs. (12) and (13) for the self and transfer inductance, respectively. One can notice that the filament solution works well only for small values of a/w, and that increasing the multipole order in general increases the dynamic range where there is agreement with the analytical solution. While the self-inductance term ΔL_1 is very well estimated when considering up to the dipole term in the first principles multipolar solution, a different situation is observed for the transfer inductance L_T, where the agreement with the bipolar solution $L_{T,bs}$ is best when using up to the octopole moment, covering a dynamic range of up to $a/w \approx 0.78$. This value is larger than what the co-location provides (about $a/w \approx 0.6$), and shows the better accuracy of the Galerkin method. These results give us the confidence that our first principles model works within the geometric characteristics of many commercial cables.

4. SQUARE AND RHOMBOIDAL ARRAYS

In this section we consider both a square array structure (with braid angle of $\alpha = 45°$ and periods of 0.179245 inches) and a rhomboidal array structure (with braid angle of $\alpha = 34.2°$) comprised of straight
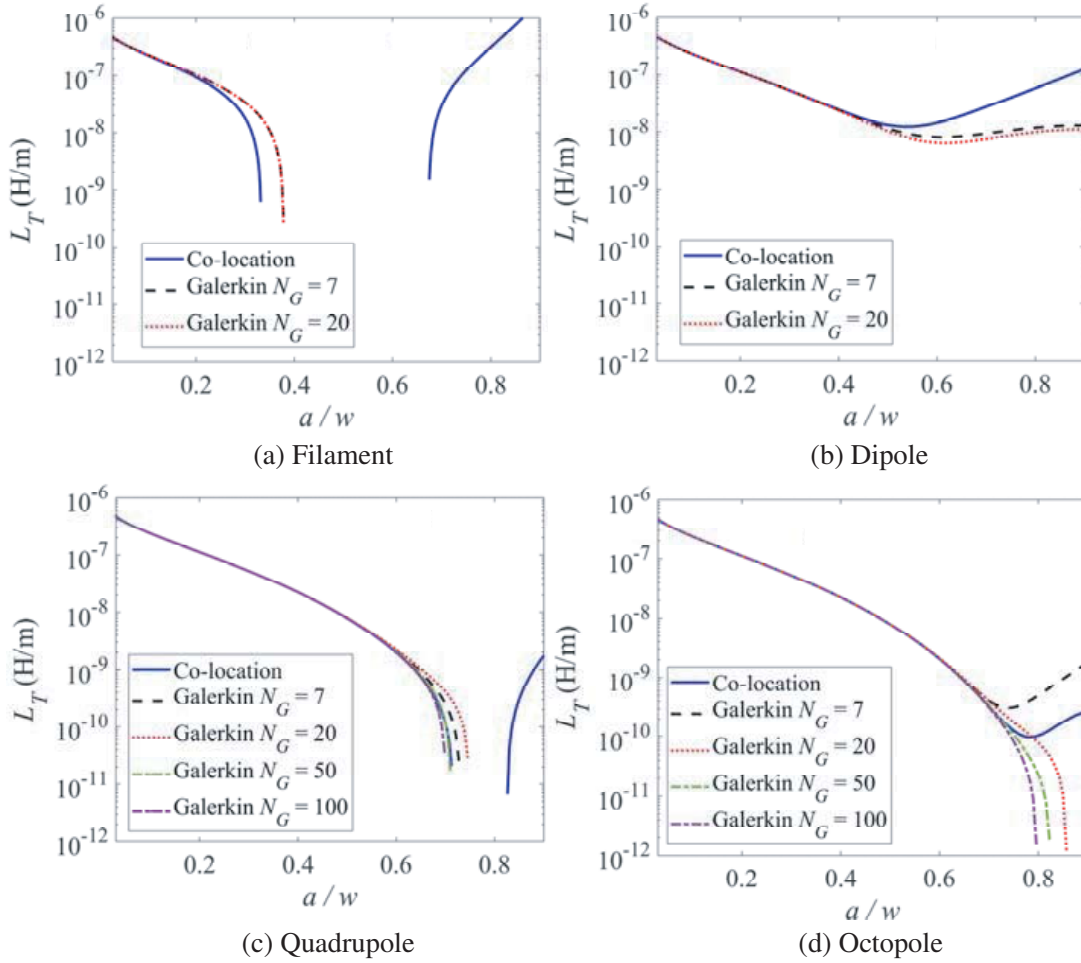
Figure 5. The transfer inductance of a one dimensional wire array versus the ratio a/w using the first principles magnetic multipole penetration model up to order (a) $M = 0$ (filament), (b) $M = 1$ (dipole), (c) $M = 2$ (quadrupole), and (d) $M = 3$ (octopole). Both the co-location and the Galerkin method are used here.

wires (with no porpoising effects) with radius 0.0025 inches as in Fig. 7. The illuminating magnetic field induces currents on the wires composing the array (equal currents in the square array case). Note that because the response of these arrays are mainly dominated by the monopole order, we use the Galerkin method with $N_G = 2$ (up to the filament) and $N_G = 3$ (up to the dipole).

We investigated the convergence with respect to the discretization of our mesh by using several discretizations in terms of number of segments per wire in the unit cell. This study is necessary to make sure we are obtaining consistent results, and a summary is reported in Fig. 8 for the transfer inductance (very similar values are calculated for the self-inductance). We observe that there is little variation in the results by increasing the number of segments per wire for a given multipole order, with the filament solution already providing an acceptable value for the array parameters.

It is instructive to analytically model the square array as the collection of two one-dimensional arrays for which we know the solutions of self- and transfer inductances, which are the same as the ones exhibited by the one-dimensional array. Comparing the multipolar results achieved for these inductances to the values estimated by the results of the one-dimensional array in Fig. 8 (dashed red line, computed as the thin-wire approximation form of $L_T = \mu_0 w \ln[w/(\pi a)]/(\pi^2 D_m)$), we find them in good agreement, verifying our first principles model. For the rhomboidal array case, a simple analytical solution is not available; however, we can use Kley's model (keeping only the contribution from $M_L = 0.875\pi\mu_0(1 - G)^3[2 - \cos(\alpha)]\exp(-\tau_h)/(6m)$ due to absence of porpoising effects, with
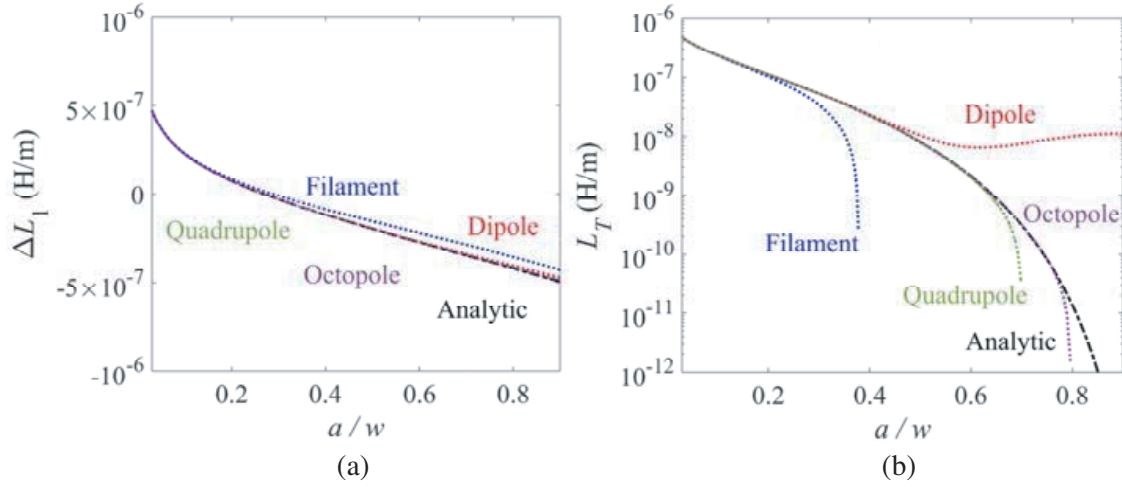
Figure 6. (a) The self and (b) the transfer inductance of a one dimensional wire array versus the ratio a/w using the first principles magnetic multipole penetration model up to order (a) $M = 0$ (filament), (b) $M = 1$ (dipole), (c) $M = 2$ (quadrupole), and (d) $M = 3$ (octopole). The Galerkin boundary condition in Eq. (6) with the largest N_G considered for each multipole order is used here. The black dashed-dotted curves are the analytical results in Eqs. (12) and (13).
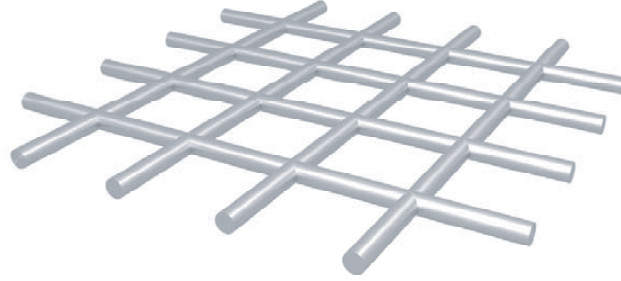
Figure 7. Schematic of a square/rhomboidal array comprised of straight wires.

$\tau_h = 0.8\tau_e$, $\tau_e = 12G(B^2 d/D_m)^{1/3}$, $B = G(2 - G)$, $G = G_0/\cos(\alpha)$, $G_0 = mnd/(2\pi D_m)$, $d = 0.005$ inch is the wire diameter, $D_m = 0.1277$ inch is the average braid diameter, $n = 1$ is the number of wires per $m = 4$ carriers) to give an estimate of the transfer inductance, also reported in Fig. 8 as a dashed red line (these formulas give $L_T = 163.9$ nH/m for the square array), in good agreement with the first principles model estimates for the rhomboidal array.

5. TWO LAYERS OF ONE-DIMENSIONAL ARRAYS OF WIRES

In this section we consider a structure comprising two layers of one-dimensional arrays of wires as in Fig. 9 in order to estimate porpoising effect. Each one-dimensional array is as in Fig. 3 (radius a and periodicity $2w$), and the distance along the y direction between the two layers is $2h$.

We consider here the two cases of $h = 2a$ and $h = 10a$, for which we develop analytical solutions for both the self and transfer inductance. These analytical solutions are based on a two-dimensional multipole-conformal mapping expansion for the wire currents. Note this multipole-conformal mapping method is valid only for the case of one-dimensional arrays of wires, while our first principles model is applicable to general cable structures.

We compare in Fig. 10 and Fig. 11 the results for the self and transfer inductance, respectively, from the first principles model considering up to the octopole moment using the Galerkin boundary condition with $N_G = 100$ to the analytical solutions from the multipole-conformal mapping expansion with $M = 1$ and $M = 7$. One can notice that, due to porpoising effects, these results are rather different
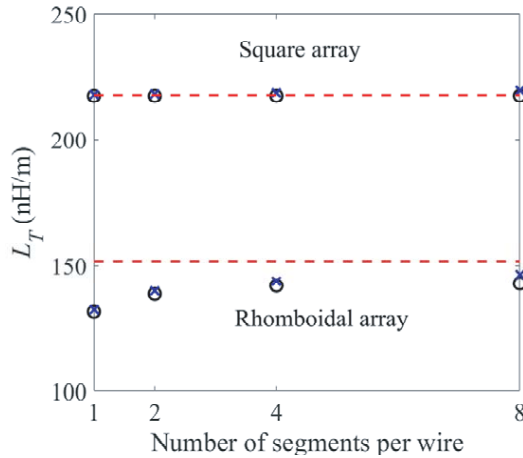
Figure 8. The values of L_T in nH/m computed using the first principles model with up to the filament (circles) and up to the dipole (crosses) for both a square array and a rhomboidal array with straight wires for several mesh discretizations. The expected results from a one-dimensional array solution (square array) and Kley's solution (rhomboidal array) are also provided as dashed red lines.
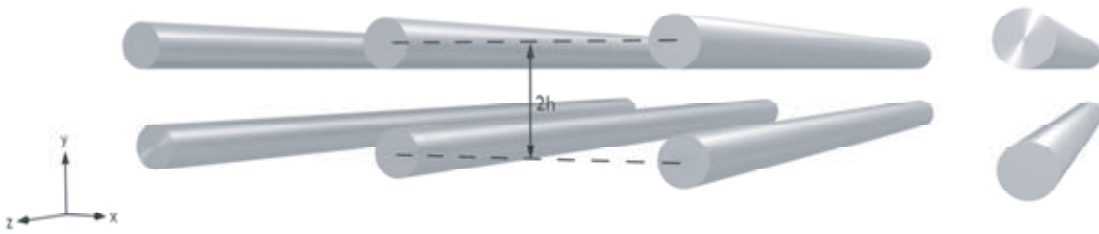
Figure 9. Schematic of a structure comprising two layers of one-dimensional arrays of wires, and the distance between the two layers is $2h$.
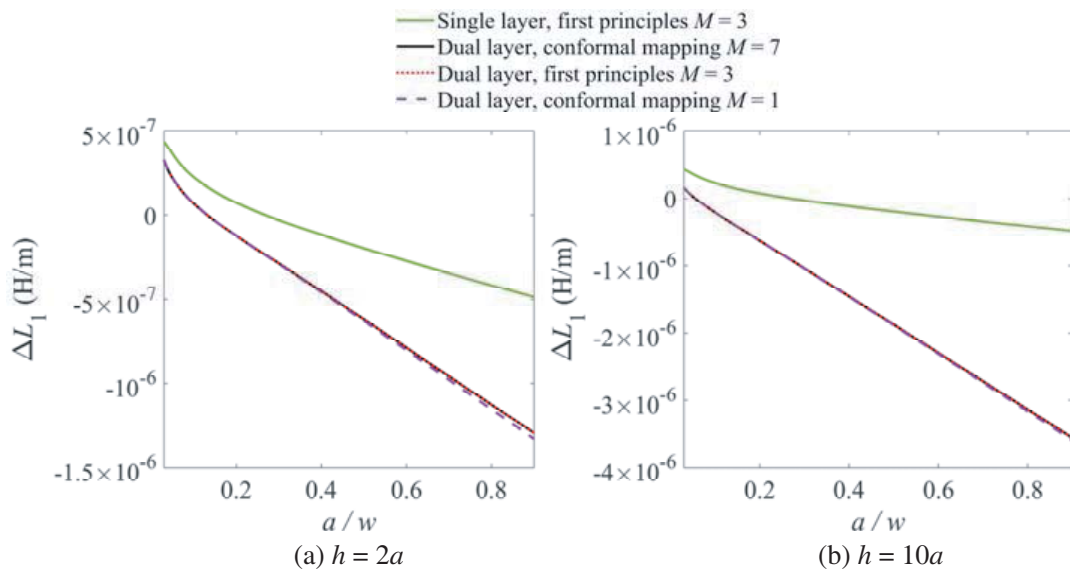
Figure 10. The self inductance of a structure comprised of two layers of one dimensional arrays of wires versus the ratio a/w using the first principles magnetic multipole penetration model up to order $M = 3$ (octopole) with $N_G = 100$ (red curve). The purple and black curves are the analytical results from the multipole-conformal mapping expansion with $M = 1$ and $M = 7$. The green solid curve is the octopole result from the first principles model in Fig. 6 for a single layer.

(a) $h = 2a$ (b) $h = 10a$
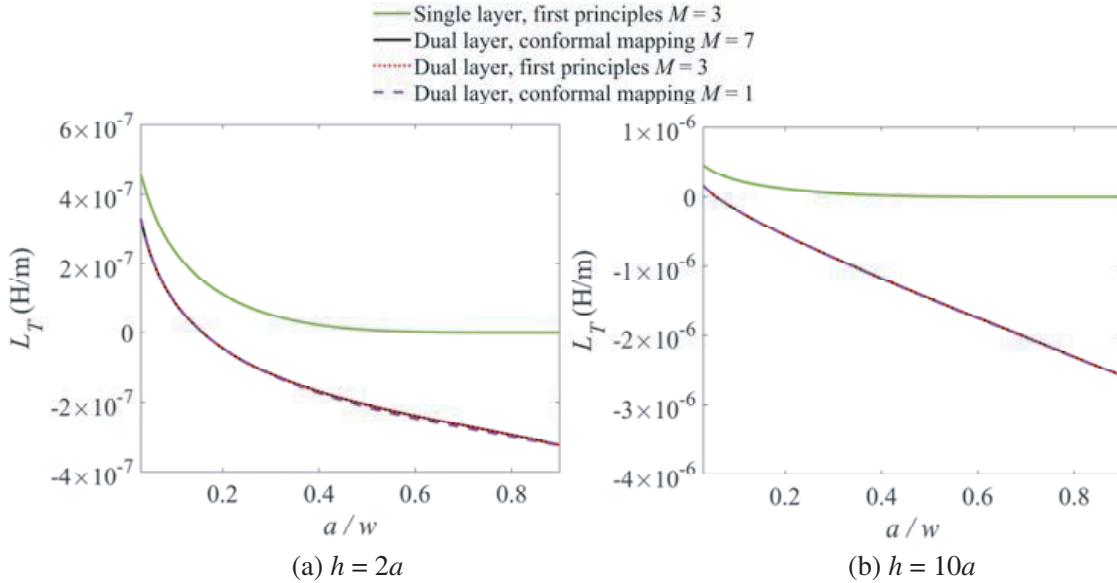
Figure 11. The transfer inductance of a structure comprised of two layers of one dimensional arrays of wires versus the ratio a/w using the first principles magnetic multipole penetration model up to order $M = 3$ (octopole) with $N_G = 100$ (red curve). The purple and black curves are the analytical results from the multipole-conformal mapping expansion with $M = 1$ and $M = 7$. The green solid curve is the octopole result from the first principles model in Fig. 6 for a single layer.

from the single layer results, and both self and transfer inductances are dominated by porpoising effects and become more negative. Good agreement with the analytical model is observed for both the self-inductance term ΔL_1 and the transfer inductance L_T of the dual layer structure, confirming that porpoising effects are well modeled in our first principles model. Because the inductances are dominated by porpoising effects, less multipoles are required for an accurate estimation (note that the two conformal mapping solutions with $M = 1$ and 7 provide almost the same result). Also, one should keep in mind that porpoising effects in realistic cable structures will be less accentuated than what is shown in this test case.

6. CONCLUSION

In this paper we have verified the magnetic penetration case of our first principles, multipole-based cable braid electromagnetic penetration model reported in [8, 9]. We have implemented two methods, namely the co-location method and the Galerkin method, and showed that the latter provides more accurate results. We have first compared the results from our model for a one dimensional array of wires to previously reported analytical solutions. These results were found in good agreement up to a radius to half spacing ratio of 0.78, within the characteristics of many commercial cables (and consistent with the validity of our electric penetration case reported in [12]). We then considered three more complex situations: a square array and a rhomboidal array with straight wires (to purposefully avoid porpoising effects) as well as a structure comprising two layers of one-dimensional arrays of wires. While for the square array we compared the results from our first principles model to the results obtained using a scaled solution of the one dimensional array results, the transfer inductance of the rhomboidal array was estimated using Kley's model. Furthermore, the structure comprising two layers of one-dimensional arrays of wires was compared to a multipole-conformal mapping expansion method. Results were found in good agreement, verifying our model. The first principles model accounts for the actual cable geometry, which is particularly useful if perturbations (such as twisting or interweave changes) exist in the geometry versus nominal commercial braid parameters.

ACKNOWLEDGMENT

REFERENCES

1. Schelkunoff, S. A., "The electromagnetic theory of coaxial transmission lines and cylindrical shields," *Bell System Technical Journal*, Vol. 13, 532–579, 1934.

2. Vance, E. F., *Coupling to Shielded Cables*, R. E. Krieger, 1987.

3. Lee, K. S. H., *EMP Interaction: Principles, Techniques, and Reference Data*, Hemisphere Publishing Corp., Washington, 1986.

4. Celozzi, S., R. Araneo, and G. Lovat, *Electromagnetic Shielding*, John Wiley and Sons, 2008.

5. Tesche, F. M., M. V. Ianoz, and T. Karlsson, *EMC Analysis Methods and Computational Models*, John Wiley & Sons, Inc., New York, 1997.

6. Tyni, M., "The transfer impedance of coaxial cables with braided outer conductor," *FV. Nauk, Inst. Telekomum Akust. Politech Wroclaw, Ser. Konfi*, 410–419, 1975.

7. Zhou, G. and L. Gong, "An improved analytical model for braided cable shields," *IEEE Transactions on Electromagnetic Compatibility*, Vol. 32, 161–163, 1990.

8. Warne, L. K., W. L. Langston, L. I. Basilio, and W. A. Johnson, "First principles cable braid electromagnetic penetration model," *Progress In Electromagnetics Research B*, Vol. 66, 63–89, 2016.

9. Warne, L. K., W. L. Langston, L. I. Basilio, and W. A. Johnson, "Cable braid electromagnetic penetration model," *Sandia National Laboratories Report*, Vol. SAND2015-5019, Albuquerque, NM, 2015.

10. Johnson, W. A., L. K. Warne, L. I. Basilio, R. S. Coats, J. D. Kotulski, and R. E. Jorgenson, "Modeling of braided shields," *Proceedings of Joint 9th International Conference on Electromagnetics in Advanced Applications ICEAA 2005 and 11th European Electromagnetic Structures Conference EESE*, 881–884, Torino, Italy, 2005.

11. Campione, S., L. I. Basilio, L. K. Warne, H. G. Hudson, and W. L. Langston, "Shielding effectiveness of multiple-shield cables with arbitrary terminations via transmission line analysis," *Progress In Electromagnetics Research C*, Vol. 65, 93–102, 2016.

12. Campione, S., L. K. Warne, W. L. Langston, W. A. Johnson, R. S. Coats, and L. I. Basilio, "Multipole-based cable braid electromagnetic penetration model: Electric penetration case," *IEEE Transactions on Electromagnetic Compatibility*, Vol. 60, No. 2, 444–452, 2017.

13. Kley, T., "Optimized single-braided cable shields," *IEEE Transactions on Electromagnetic Compatibility*, Vol. 35, No. 1, 1–9, 1993.

14. Warne, L. K., K. O. Merewether, and W. A. Johnson, "Approximations to wire grid inductance," *Sandia National Laboratories Report*, Vol. SAND2007-8116, Albuquerque, NM, 2008.